

# Modal analysis of a beam with a metamaterial segment produced using additive manufacturing technology

Tomasz Ciborowski<sup>1\*</sup> , Erwin Wojtczak<sup>1</sup> , Magdalena Rucka<sup>1</sup> 

<sup>1</sup> Department of Mechanics of Materials and Structures, Faculty of Civil and Environmental Engineering, Gdańsk University of Technology, ul. Narutowicza 11/12, 80-233 Gdańsk, Poland

\* Corresponding author's e-mail: [tomasz.ciborowski@pg.edu.pl](mailto:tomasz.ciborowski@pg.edu.pl)

## ABSTRACT

The paper focuses on the analysis of the dynamic response of the mechanical metamaterials manufactured using 3D printing technology. A modal analysis of a cantilever beam with a metamaterial segment was conducted to evaluate the influence of the segment geometry on the dynamic parameters of the structure, such as natural frequencies and mode shapes. A method allowing to include the effect of the actual stiffness of the beam support in the numerical model using elastic constraints was also proposed. The significant influence of the geometry of the metamaterial segment on the dynamic behaviour of the tested beam was proved. The research findings provided new insights that are significant for potential applications of metamaterials in civil engineering.

**Keywords:** mechanical metamaterial, additive manufacturing, re-entrant geometry, experimental modal analysis, numerical simulations.

## INTRODUCTION

Metamaterials are relatively new solutions that are increasingly being applied in various scientific fields. They are defined as materials with non-classical mechanical [1,2], electromagnetic [3,4], acoustic [5–7], optical [8] or thermal [9] properties, primarily resulting from their internal structure rather than the material from which they are made. The concept of metamaterials was proposed by Vesalego [10], who characterized materials with negative dielectric constant and magnetic permeability. Research on metamaterials covers a wide range of structure types and properties, such as the influence of internal geometry on structural stiffness or the phenomenon of negative stiffness [2]. Auxetic materials, as a subgroup of mechanical metamaterials, exhibit a negative Poisson's ratio [1, 11]. Their unique properties include increased indentation resistance, better energy absorption, vibration damping capabilities, and the ability to form double-curvature surfaces for constructing objects with unusual shapes. Mechanical metamaterials have been investigated by many researchers,

mostly in terms of appropriate design of their internal structure and performance under different loads. Some examples of the current state-of-the-art are reported below. Kadic et al. [12] studied a theoretically ideal pentamode mechanical metamaterial and approximated its structure by producing physical models using three-dimensional optical lithography. The samples were tested to determine the elastic properties, namely bulk and shear modulus. Wang and Hu [13] characterized the mechanical properties of auxetic metamaterials, considering different geometries, i.e. re-entrant, rotating, nodule and fibril, and chiral structures. They reported potential applications of these configurations in textiles for smart bandages. A novel concept was presented by Neville et al. [14], who presented metamaterial produced using kirigami design principles. They proposed to form PEEK film into cellular honeycomb metamaterial by a series of cutting and folding. The prepared samples were experimentally tested to obtain elastic moduli and Poisson's ratios. Finite element simulations were also performed to predict elastic parameters. Xiao et al. [15] characterized the shrinkage of re-entrant

hexagonal honeycomb block under quasi-static and dynamic compression. They considered metallic auxetic metamaterial using theoretical calculations and finite element simulations. The results showed that the traditional approach based on the stress-strain curve underestimates the compressive strength of the structures.

The advanced development of electronic manufacturing techniques, particularly 3D printing technology, has played a crucial role in metamaterial research. 3D printing enables the precise fabrication of complex geometric structures while maintaining specific mechanical properties. Studies have shown that controlling material microstructure allows for the design of complex functional properties, including multi-material printing. Wang et al. [16] investigated additively manufactured patient-specific tissue-mimicking phantoms. They indicated that typical 3D printed phantoms do not appropriately reflect the behaviour of soft tissues under large deformations. They proposed dual-material phantoms consisting of an elastic matrix with a stiffer insert with different geometries, i.e., sinusoidal wave, double helix, and interlocking chains. Kolken et al. [17] designed additively manufactured meta-biomaterials with auxetic and conventional mechanical properties, such as hybrid elements linking both types. The samples were fabricated from a biomedical titanium alloy using selective laser melting. Simple metamaterial blocks and hip stem samples were subjected to compression tests and characterized with digital image correlation technique to evaluate elastic constants and deformation under load. Krolikowski et al. [18] compared the mechanical performance of dog-bone samples produced from TPU rubber-like material with and without metamaterial segments under tension. They compared stress-strain curves from experiments and numerical simulations, and characterized stress distribution in the samples. A comprehensive review of additive manufactured meta-biomaterials has been carried out by Zadpoor [19]. The author characterized the typical mechanical properties of meta-biomaterials, the challenges in 3D printing of these structures and the fatigue behaviour with respect to potential applications. Another review on 3D printed metamaterials was performed by Dogan et al. [20]. The authors reported on the application of mechanical metamaterials in tissue engineering in the aspect of different manufacturing techniques. The issue of different metamaterial configurations and their specific properties has been considered,

including increased stiffness, auxetic properties, high toughness and super-elasticity. Yang and Ma [21] designed axisymmetric auxetic metamaterials obtained by rotating a two-dimensional lattice with double-U and re-entrant geometry. The cylinders were produced using different techniques, i.e., fused filament deposition, stereo-litography and digital light procession, and subjected to compression tests. The elastic constants were identified for different geometries of lattices. Li et al. [22] proposed a hybrid metamaterial consisting of an additively manufactured lattice filled with polyurethane foam. Different configurations of lattice were considered, i.e., hyperbolic, body-centered cubic, and hexaround face-centered. Experimental tests and numerical simulations were performed to evaluate the performance of such dual-material samples under low-velocity impact test. The proposed hybrid metamaterials achieved better energy absorption than pure lattice or pure foam, and also longer elastoplastic and damage evolution stages.

An important aspect of metamaterial research is the analysis of their dynamic behaviour. Studies have been conducted on the dynamics of hexagonal gradient structures, which may lead to the design of materials with optimal mechanical and dynamic properties. The behaviour of structures under dynamic loading has also been analysed, which is crucial for materials used in extreme loading conditions (e.g. seismic). Boldrin et al. [23] reported the results of a vibroacoustic analysis of an auxetic gradient honeycomb composite with hexagonal configuration. The authors performed modal analysis using laser vibrometry on additively manufactured samples. They obtained a good agreement between experimental tests and numerical simulations using a finite element method. Mazloomi et al. [24] performed vibroacoustic tests on sandwich panels with a core of auxetic hexagonal honeycomb in 2D. They performed numerical simulations on a homogenized finite element model and on a full-scale detailed model. In both cases, the mode shapes and natural frequencies were determined and good agreement was obtained. One of the aspects of the dynamic behaviour of mechanical metamaterials is their use in the reduction of vibrations of other structures. Anigbogu et al. [25] used a metamaterial structure as a layered beam for attenuation of vibrations. Based on the theoretical model of a layered metamaterial beam, the authors showed that the metamaterial design can affect different frequency ranges differently. They also fabricated a metamaterial sample and experimentally

verified its effectiveness. Pires et al. [26] presented different solutions of locally resonant metamaterials. They experimentally evaluated their potential in suppressing flow-induced noise and vibration of a plate, proving the efficiency of the proposed approach. The above reported works prove that mechanical metamaterials are popular throughout the researchers, however, the analysis of dynamic behaviour of structures with metamaterial inserts has not been fully investigated.

In this study, the dynamic behaviour of an additively manufactured beam with an embedded metamaterial segment was investigated, with the focus on the influence of the internal geometry of the metamaterial on the dynamic properties of the system. The re-entrant geometry was chosen due to its high energy absorption dissipation, high specific stiffness and effectiveness in tuning the dynamic response. These structures also offer improved control over directional mechanical properties and are easier to fabricate using 3D printing, making them a more practical solution. Several variants of the segment with different geometries were analysed using numerical calculations with the finite element method. A physical model was additively manufactured for a selected geometric configuration and subjected to experimental modal analysis. A numerical model of the tested beam was also produced. The aim was to demonstrate that by tailoring the internal geometry of the metamaterial, it is possible to achieve the desired dynamic characteristics of the structure.

## MATERIALS AND METHODS

### Parametric analysis

#### Object of the research

The initial studies were performed on a cantilever beam made of polylactic acid (PLA), with

the material parameters determined in a tensile test: Young's modulus  $E = 2.580$  GPa, Poisson's ratio  $\nu = 0.36$  [-], and mass density  $\rho = 1175.9$  kg/m<sup>3</sup>. The beam had a cross-section of  $30 \times 30$  mm<sup>2</sup> and a length of 150 mm. The metamaterial segment had dimensions of  $30 \times 30 \times 30$  mm<sup>3</sup> and accounted for one-fifth of the total beam span. It was positioned at a distance of 90 mm from the beam support (Figure 1).

The metamaterial segments were based on a re-entrant geometry. The axial dimensions of the single cell were initially set, assuming a height of  $a = 5$  mm and a width of  $b = 10$  mm (Figure 2b). The width of the cell varied depending on the wall thickness (Figure 2c) to achieve a structure composed of three cells across the width with a total width of 30 mm (Figure 2a). The analysed structures differed in two variables: wall thickness  $d = (0.6, 0.7, 0.8, 0.9, 1.0)$  mm and the internal angle defined by  $\theta = (-15, -10, -5, 0, 5, 10, 15)^\circ$ . Structures with negative and positive angles were analysed to exhibit classical and auxetic properties, respectively. To minimize local stress concentrations, the cell vertices were rounded (Figure 2c).

### Numerical calculations

The parametric analysis of the influence of the segment geometry on the behaviour of the beam was conducted based on the theoretical modal analysis using the Abaqus environment. Reduced integration solid elements (C3D8R) were employed. The discretisation was determined through a convergence analysis, using the values of the first three natural frequencies as the convergence criterion. The finite element mesh size in the metamaterial segment was 0.5 mm, while in the beam section outside the segment, it was 1.0 mm (Figure 3). A homogeneous, isotropic, linear elastic material model was assumed with constants given in Section Object of the research.

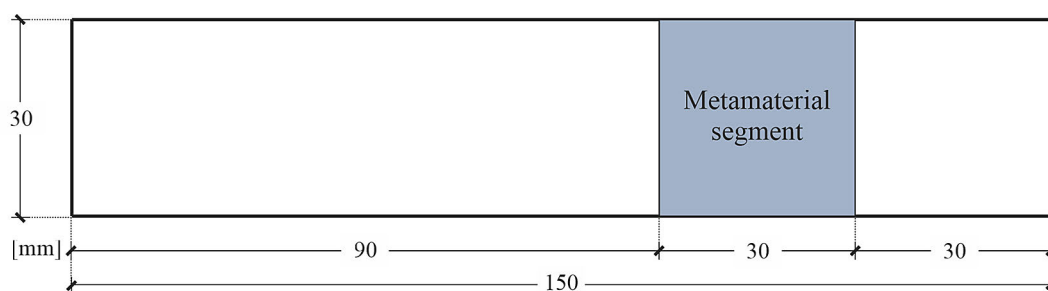


**Figure 1.** Geometry of the analysed beam with a metamaterial segment (side view)

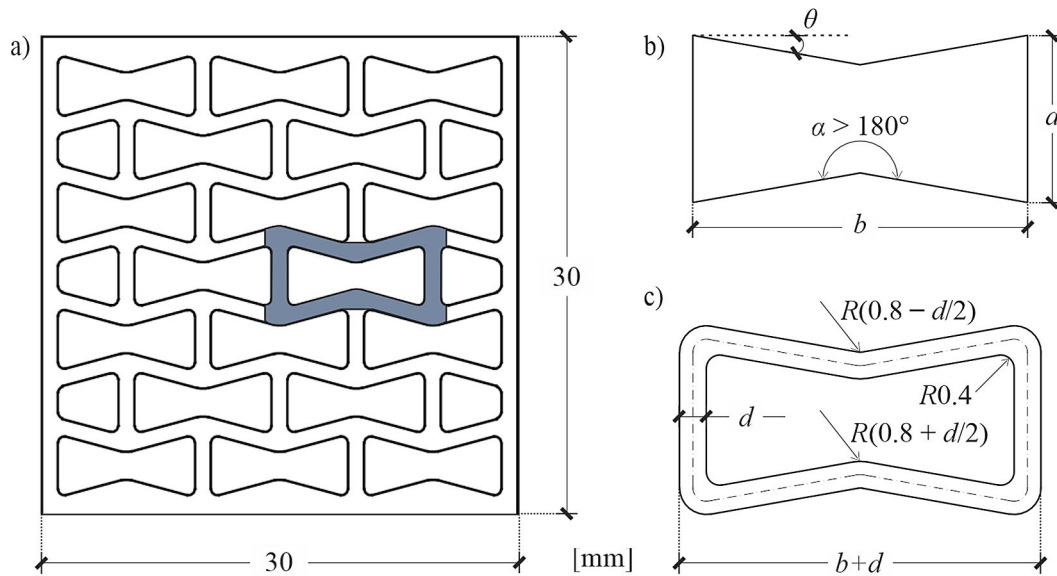


**Figure 2.** Metamaterial structure: (a) a cross-section of the segment, (b) re-entrant geometry (axial dimensions) with a positive angle  $\theta$  and an internal angle  $\alpha > 180^\circ$ , (c) a single symmetric segment cell with a wall thickness  $d$  and corners rounded with radius  $R$

The beam analysis was performed for a statically determinate cantilever beam configuration (one end was fixed while the other remained free). The metamaterial segment was modelled as a separate part connected to the remaining solid parts of the beam using *Constraint-Tie* module, connecting all translational degrees of freedom. A linear frequency analysis was adopted. The first ten natural frequencies and their corresponding mode shapes were determined. The results obtained allowed for the assessment of the effect of changes in the segment wall thickness and the measure of the internal angle on the modal parameters of the beam.

**Modal analysis of the selected beam**

*Description of the physical model*

The further analyses were performed on a beam with a metamaterial segment of geometry selected based on the parametric analysis, specifically with a wall thickness  $d = 0.8$  mm and an angle  $\theta = 10^\circ$ . The metamaterial segment of the beam had an externally visible structure (Figure 4). The beam was produced using additive manufacturing technology (FFF – fused filament fabrication approach) on a Raise3D E2 printer. PLA21 filament with a diameter of 1.75 mm and a tolerance of 0.05 mm was used. The beam with a total length of 180 mm was printed, exceeding the theoretical length by 30 mm to allow appropriate mounting during experimental tests. The

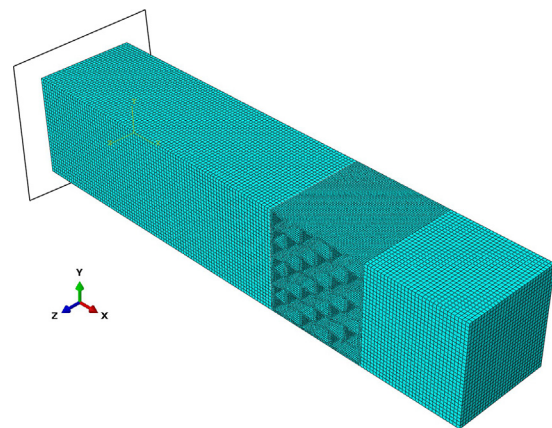


**Figure 3.** Adopted discretization in the finite element model

beam was printed in a horizontal orientation, with layers deposited along its longitudinal axis. This direction was selected to ensure consistent material behaviour along the primary axis of bending and to minimize anisotropic effects often associated with the FFF technique.

To appropriately reflect the stiffness of the beam, it was necessary to determine an effective Young’s modulus under bending which allowed including the influence of the particular printing direction of the element. For this purpose, a three-point bending test was performed on a Zwick/Roell Z100 universal testing machine (Figure 5). The distance between the supports was set as 160 mm. The beam was initially loaded with 50 N and then,

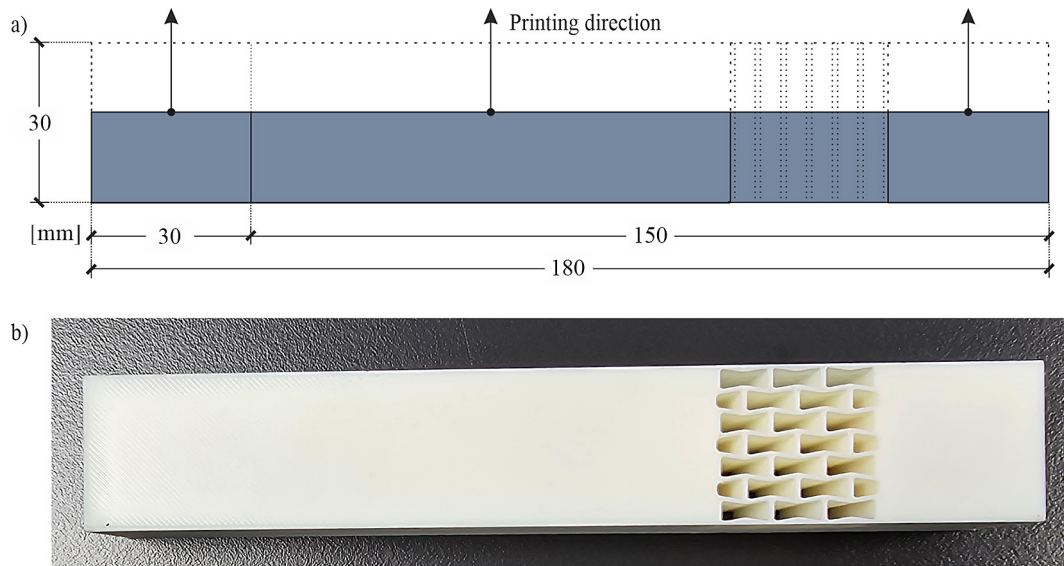


**Figure 4.** The selected beam with a segment adopted for experimental testing ( $d = 0.8$  mm,  $\theta = 10^\circ$ ): (a) printing direction, (b) a photograph of the printed beam

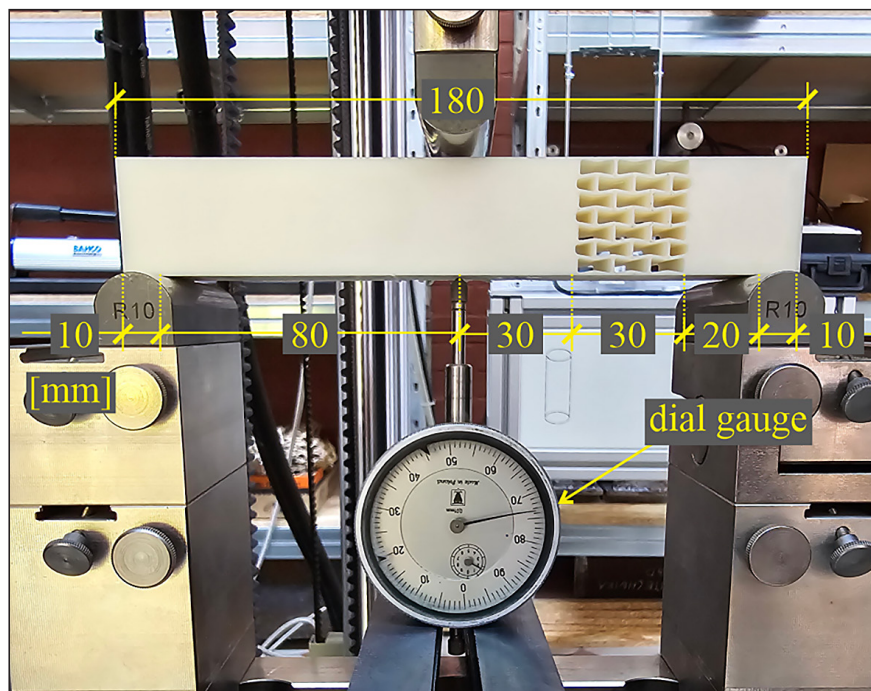


**Figure 5.** Three-point bending test performed using Zwick universal testing machine

the test was performed at a constant displacement rate of 0.5 mm/min in the linear elastic region. The force value and the displacement were measured during the whole test. The test was finished at a given displacement of 0.5 mm, for which the linear relation between force and displacement was maintained. A dial gauge was placed under the beam to measure the actual deflection, in order to exclude the compliance of the test machine elements. The increase in the bending force

registered by the machine during the whole test and the displacement measured by the dial gauge were further used to calibrate the results. Since the beam did not satisfy classical beam theory, the effective elastic modulus was determined based on the calibration of the theoretical results from the Abaqus program with the experimental ones. The numerical model reflecting the actual geometry of the beam was created. A series of calculations with different values of Young's modulus

were performed and the bisection technique was used to determine the optimal value. The obtained Young’s modulus was  $E = 2.96$  GPa, which was higher than the one determined using tensile tests due to the particular geometry of the structure and the specificity of the manufacturing process.

*Experimental modal analysis*

The experimental setup consisted of the beam secured in metal clamps and the measuring equipment (Figure 6a). The analysis was conducted using an impulse test generated by a modal hammer 086C03 with a sensitivity of 2.25 mV/N, within a measurement range of  $\pm 2224$  N and a resonance frequency of  $\geq 22$  kHz. The vibrating structure

enabled direct recording of acceleration value over time using a three-axis ICP accelerometer 356A15, with the following parameters: sensitivity of 10.2 mV/(m/s<sup>2</sup>), measurement range of  $\pm 490$  m/s<sup>2</sup>, resonance frequency of  $\geq 22$  kHz, and frequency range of 2–5000 Hz. The sensor, equipped with a magnet, was attached to a steel pad adhesively bonded to the bottom surface of the beam at its free end. The force was applied with the modal hammer vertically (along Z direction) at various locations on the upper surface of the beam while accelerations were measured simultaneously in three perpendicular directions: X, Y, and Z, consistently at the same fixed point. The recorded signals were obtained using a portable LMS SCADAS Mobile system. A total of 75 individual measurements

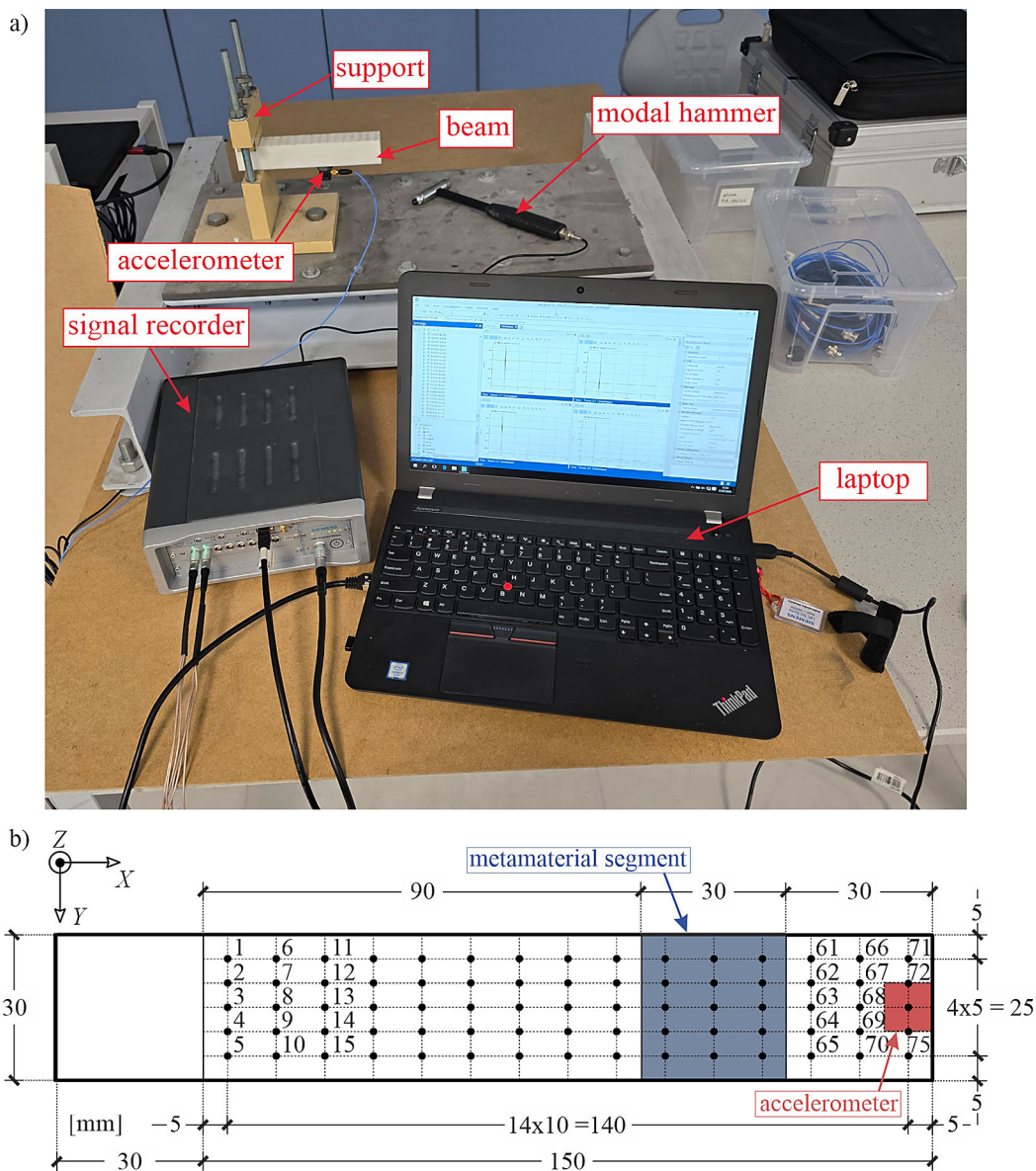


**Figure 6.** Experimental modal analysis: (a) support and measuring equipment, (b) measurement points

were conducted (Figure 6b). The sought quantities, namely natural frequencies and mode shapes, were estimated using the frequency response function – FRF (particularly, the accelerance), calculated as a ratio of output acceleration signals to input force signal. The natural frequencies were identified as peak values in the FRFs, whereas the mode shapes were determined based on the peak amplitudes of the imaginary part of the FRFs.

### Numerical modal analysis

The numerical model was prepared similarly to that described in section Description of the physical model. To accurately reflect the experimental conditions, the mass of the accelerometer and the attached pad were modelled as a rectangular prism with material parameters characteristic of steel (Figure 7a). The elastic modulus was updated to the value determined in section Experimental modal analysis from the calibration with the static three-point bending test. The actual length of the beam (180 mm) was modelled,

while the theoretical length remained at 150 mm. Due to the difficulties in achieving a fixed mounting of the beam in the clamps during the experiment, the fixed support was replaced with elastic constraints attached to the end part of the beam at the length of 30 mm, resulting in the previously assumed theoretical length of 150 mm. Elastic constraints differing in stiffness  $k$  were provided in two directions: vertical  $k_1$  and lateral  $k_2$ , assuming that  $k_1 \geq k_2$ , since the clamps were mostly fixing vertical direction (Figure 7b-d). The constraints were applied to all nodes on four surfaces, each with the area of  $30 \times 30 \text{ mm}^2$ , providing elastic support with finite stiffness (Figure 7c). The movement of the beam along its axis was fixed. During the calculations, the values of the stiffness in both directions ( $k_1, k_2$ ) were manipulated to calibrate the numerical frequencies with the experimental ones. A solid beam of the same size was adopted as a comparative model to show the influence of the presence of the chosen meta-material segment.

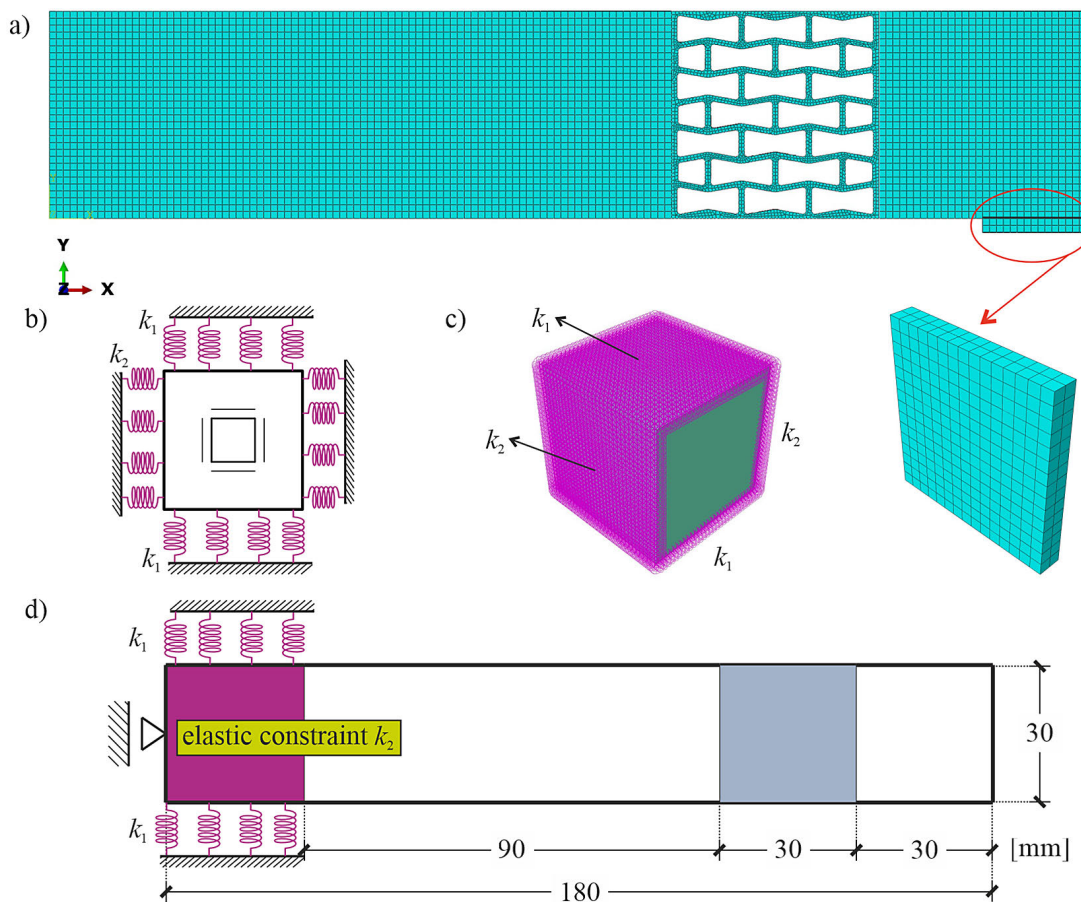


**Figure 7.** Numerical model of the selected beam: (a) FEM model of beam with an accelerometer, (b) model of the mounting of the measurement stand – elastic constraints in two directions, (c) elastic constraints applied on the part of the beam in Abaqus, (d) side view of the beam

## RESULTS AND DISCUSSION

### Parametric analysis

The values of the natural frequency of the beam with a metamaterial segment, depending on the wall thickness of the segment and the internal angle, are presented below in Tables 1–4. Figure 8 shows the graphical representation of the data given in the tables, the representative examples of mode shapes for  $d = 0.8 \text{ mm}$  and  $\theta = 10^\circ$  are

also presented. The first frequency (Table 1, Figure 8a) corresponds to the vertical bending mode, where higher values occur for negative angles, as the convex structure exhibits better bending resistance. The second frequency (Table 2, Figure 8b) is related to the lateral bending mode, with the highest frequencies observed at an intermediate angle of  $0^\circ$ , as the inclined arms of the metamaterial cells deform at other angles. The third frequency (Table 3, Figure 8c) corresponds to the second vertical bending mode, showing a trend

**Table 1.** Values of the first natural vibration frequency of the beam depending on the wall thickness and the measure of the internal angle

$d$ [mm]	$\theta$ [°]							Trend
	-15	-10	-5	0	5	10	15	
0.6	190.26	152.73	144.61	61.745	83.86	97.73	96.193	
0.7	292.05	243.33	265.09	244.03	202.34	194.82	225.21	
0.8	304.55	295.43	285.52	271.15	266.32	251.83	251.72	
0.9	313.11	306.49	299.18	288.80	284.32	277.48	272.23	
1.0	318.25	308.77	299.18	301.70	297.47	291.88	287.55	
Trend								

**Table 2.** Values of the second natural vibration frequency of a beams in parametric analysis depending on wall thickness and the measure of the internal angle

$d$ [mm]	$\theta$ [°]							Trend
	-15	-10	-5	0	5	10	15	
0.6	323.31	326.46	328.97	329.56	328.52	325.01	321.00	
0.7	326.86	328.93	331.25	331.8	330.96	328.65	326.63	
0.8	328.55	330.69	332.30	332.8	332.43	329.47	328.26	
0.9	329.57	331.38	332.76	333.19	332.57	331.17	329.09	
1.0	330.02	330.47	332.76	333.17	332.66	331.28	329.40	
Trend								

**Table 3.** Values of the third natural vibration frequency of a beams in parametric analysis depending on wall thickness and the measure of the internal angle

$d$ [mm]	$\theta$ [°]							Trend
	-15	-10	-5	0	5	10	15	
0.6	857.02	832.48	819.68	527.92	728.96	747.36	753.72	
0.7	1143.6	964.18	1034.8	971.88	887.68	878.96	923.44	
0.8	1217.6	1167.6	1117.2	1056.1	1037.6	989.29	987.74	
0.9	1285.0	1241.0	1195.1	1135.4	1115.3	1083.3	1061.2	
1.0	1339.8	1247.4	1195.1	1216.6	1193.9	1161.8	1139.4	
Trend								

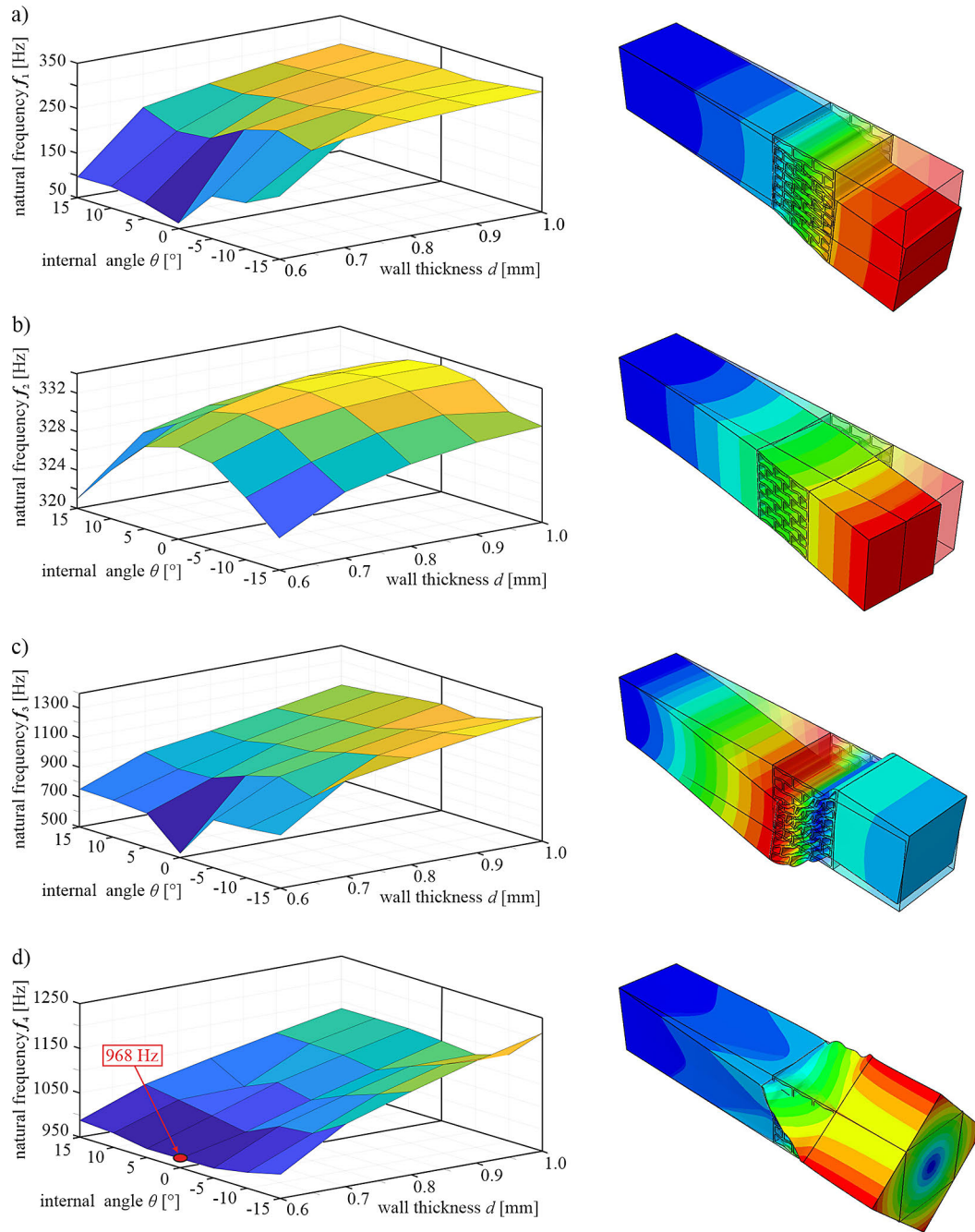


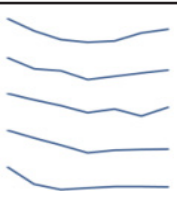
**Figure 8.** The change of the first four natural frequencies of the beam with metamaterial segment and example of mode shapes for  $d = 0.8$  mm and  $\theta = 10^\circ$ : (a) mode 1 (vertical bending), (b) mode 2 (lateral bending), (c) mode 3 (vertical bending), (d) mode 4 (torsion)

consistent with the first frequency. The fourth frequency (Table 4, Figure 8d) is related to the torsional vibration mode, where the pattern reverses compared to the second frequency: the lowest values occur at  $0^\circ$ .

The influence of the wall thickness  $d$  on the results is also significant. In general, the lowest frequencies were obtained for the wall thickness equal to  $d = 0.6$  mm, indicating possible local vibrations in this case. The influence of the

wall thickness can be clearly demonstrated by the comparison of mode shapes for metamaterial with constant angle  $\theta$  but with varying  $d$ . Figure 9 shows the third mode shape for  $\theta = -10^\circ$  and the wall thicknesses equal to 0.6, 0.7, and 0.8 mm. It can be observed that thinner walls are related to lower structural stiffness of the metamaterial segment and significant deformation in its area compared to the remaining part of the beam. As the wall thickness increases, this effect is reduced and

**Table 4.** Values of the fourth natural vibration frequency of a beams in parametric analysis depending on wall thickness and the measure of the internal angle

$d$ [mm]	$\theta$ [°]							Trend
	-15	-10	-5	0	5	10	15	
0.6	1004.3	985.63	972.20	<b>968</b>	970.24	982.61	988.09	
0.7	1091.4	1047.2	1040.1	<b>1004.4</b>	1018.2	1030.9	1042.8	
0.8	1137.8	1108.7	1082.9	1049.7	1066.7	1034.2	1075.2	
0.9	1180.6	1149.2	1122.3	1090.5	1101.7	1104.5	1105.5	
1.0	1216.1	1144.9	1122.3	1129.6	1135.0	1134.9	1134.1	
Trend								

the mode shape becomes smoother. What is also worth noting, the other mode shapes can correspond to purely local deformation without significant vibration of the entire beam (Figure 9d). An increase in the wall thickness consistently resulted in an increase in natural frequencies, suggesting that the change of the wall thickness has a more significant influence on the structural stiffness than on its mass. The highest frequencies were obtained for  $\theta = -15^\circ$  and  $d = 1.0$  mm, indicating that the convex geometry of the cell and the increase in wall thickness contribute to the stability of the dynamic parameters, which is intuitive.

From the fourth mode of vibration onwards, significant disturbances in the mode shapes occur, making it difficult to match specific natural frequencies obtained for different geometric configurations. This is related to the above-mentioned local vibrations in metamaterial segment,

particularly much more pronounced in segments with thinner walls, specifically 0.6 mm and 0.7 mm (Table 4, bolded values). Considering the maximization of natural frequencies, the wall thickness equal to  $d = 1.0$  mm and the angle  $\theta = -15^\circ$  should be regarded as the most advantageous geometric configuration. However, some other factors need to be considered while choosing an optimal geometry. The analysis showed that segments with  $\theta = 10^\circ$  provide balanced ratios between the frequencies of individual modes, thus these segments offer a good balance between different types of vibrations. Furthermore, the angle of  $10^\circ$  is related to the auxetic properties of the metamaterial segment, which is an important feature for obtaining increased stiffness while maintaining relatively low mass. It is also noteworthy that the wall thickness  $d = 0.8$  mm provide the stabilization of the frequency variation

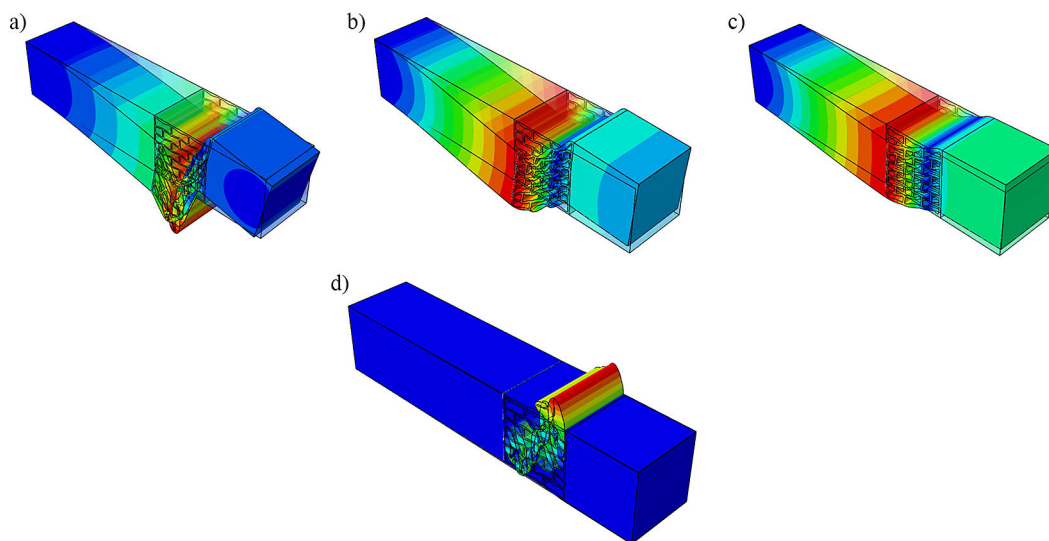


**Figure 9.** The effect of small low thickness on the presence of local vibrations in the beam: the third mode for angle  $\theta = 10^\circ$  and wall thickness equal to 0.6 mm (a), 0.7 mm (b), and 0.8 mm (c); example of higher mode shape with visible local vibrations of the metamaterial segment with  $\theta = 10^\circ$  and  $d = 0.6$  mm (d)

(the trend line becomes smooth). Additionally, no local vibrations in the structure were observed for segments at this thickness. The segments with thinner walls experience the local stress concentrations during deformation, while the segments with thicker walls gain more mass, which is undesirable. Moreover, the metamaterial segment with thinner walls could be more challenging to produce using 3D printing technology. Therefore, for further analyses, a segment with the wall thickness of  $d = 0.8$  mm and the measure of the internal angle  $\theta = 10^\circ$  was selected.

### Modal analysis of the selected beam

#### Experimental modal analysis

Based on the results of the experimental modal analysis, the values of the natural frequencies and their corresponding mode shapes were identified. Analysing the Fourier transforms, it was observed that only a few distinct peaks were visible in the

frequency spectra. The subsequent peaks were unclear and difficult to interpret. This effect may be attributed to several factors, such as weaker excitation of higher frequencies during the experiment related to the high damping of the material, which could lead to lower response amplitudes. Five initial natural frequencies and the corresponding mode shapes were determined for the beam (Figure 10). Certain disturbances were observed in the identified mode shapes, which may result from inaccuracies in the excitation process using the modal hammer. It was noted that some mode shapes (first and fourth, Figure 10a, d) exhibited characteristics atypical for cantilevers, such as a lack of tangency to the initial longitudinal axis of the beam in the fixed support area. The observed effect indicates that these eigenmodes were related to the vibrations of the tested beam with the measurement stand, suggesting that components of the measurement setup are susceptible to vibrations. For this reason, only the second, third and fifth

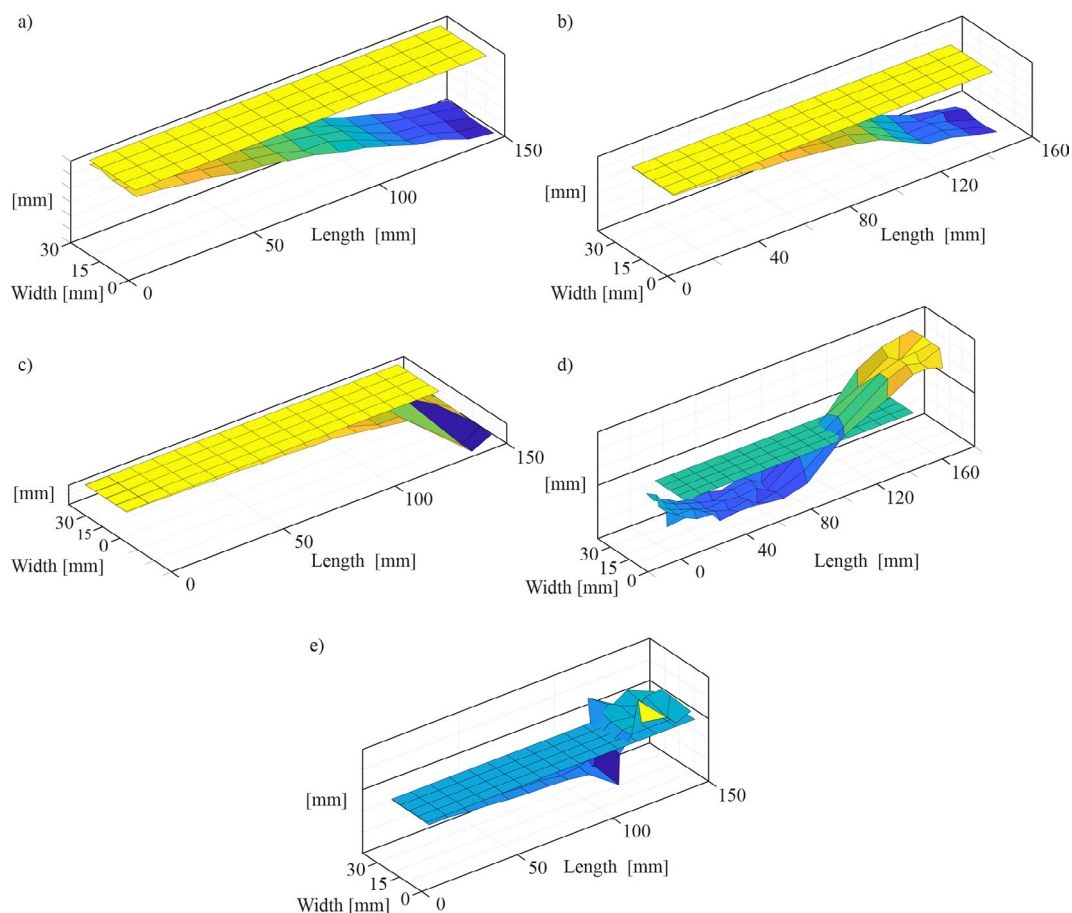


**Figure 10.** Experimental mode shapes: (a) mode shape #1 ( $f = 107.2$  kHz): vibrations of the measurement stand, (b) mode shape #2 ( $f = 176.1$  kHz): first bending mode (vertical), (c) mode shape #3 ( $f = 186.8$  kHz): lateral bending mode, (d) mode shape #4 ( $f = 386.2$  kHz): vibrations of the measurement stand, (e) mode shape #5 ( $f = 760.6$  kHz): second bending mode (vertical)

mode shapes (Figure 10b, c, e) could be considered as typical for vibrations of the beam itself. It is also important to note that the last mode (Figure 10e) exhibits significant disturbances, that could result from the sensitivity of the conducted impulse test to inaccuracies in the excitation of the vibrations in the higher frequency range.

*Numerical modal analysis*

As the first part of the numerical analysis, the elastic constraints were selected iteratively to ensure the agreement with the experimental results. Since only two mode shapes could be reliably identified from the experiment, they were used as indicators of the compatibility. The obtained spring constants for the two directions were as follows:  $k_1 = 180 \text{ N/mm}$  and  $k_2 = 55 \text{ N/mm}$ . Then, the results of the modal analysis, i.e., the two initial natural frequencies and mode shapes were determined. To illustrate the effect of introducing the metamaterial segment, the results were compared with the frequency values for the solid beam, without the segment (Table 5, Figure 11). It can be seen that the lateral bending mode

has a lower frequency than the vertical bending mode, which is the results of different stiffness of the elastic constants in the horizontal and vertical directions. A clear reduction in the natural frequencies between the solid beam and the beam with the metamaterial segment indicates a significant influence of the segment on the modal properties. The vertical bending mode has almost 30% lower frequency, whereas the lateral bending mode experiences approximately 15% decrease. This difference results from the fact that metamaterial segment changes structural stiffness of the beam in both directions differently. Figure 11 shows that the vertical bending mode is much more affected by the presence of the metamaterial segment than the lateral bending mode. The decrease in the natural frequencies can be interpreted as the result of local stiffness weakening in the region where the metamaterial segment is introduced. This modification leads to increased local deformations and alters the way vibrations propagate throughout the beam. This effect is especially pronounced in lower modes, which typically represent more global deformation patterns.

**Table 5.** Comparison of natural frequencies between numerical results (the solid beam and the beam with a segment) and the difference experimental beam

Mode shape	Numerical results			Experimental results [Hz]	Relative error [%]
	Solid beam [Hz]	Beam with metamaterial [Hz]	Frequency difference [%]		
Vertical bending	247.92	174.90	29.45	176.10	0.68
Lateral bending	216.34	184.84	14.56	186.80	1.05

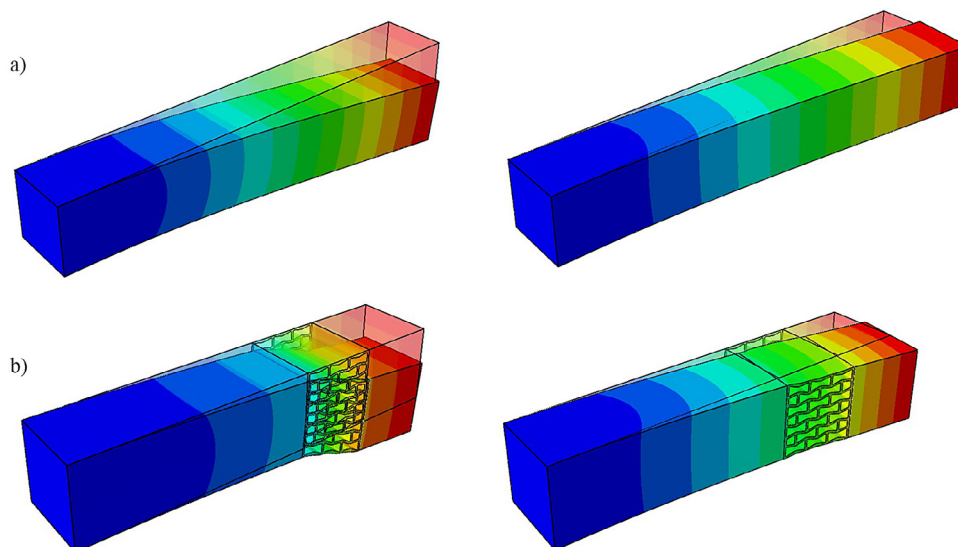


**Figure 11.** Comparison of the first vertical bending (left column) and first lateral bending (right column) natural mode shapes from numerical simulations for: (a) solid beam, (b) beam with metamaterial segment

A comparison of experimental and numerical results is presented in Table 5. The differences in results do not exceed 1.5%, however, it should be noted that this correlation is verified only for the first two vibration modes due to the previously mentioned difficulties in identifying higher natural frequencies from experimental data.

## CONCLUSIONS

The paper presents the results of the modal analysis of the beam structure with a metamaterial segment operating in a cantilever beam configuration. The numerical approach allowed to analyse the influence of the geometric parameters of the metamaterial segment on the dynamic response of the structure. Based on the observations of the vibration modes, the optimal variant of the segment was selected. A significant impact of the printing direction of the beam on its mechanical properties was observed; therefore, a static bending test was conducted. By comparing the obtained deflection results from both the experiment and the numerical model, the effective Young's modulus of the material under bending was determined.

The results of the experimental measurements revealed a significant influence of the static scheme of the measurement setup on the results obtained. The vibration modes were not only influenced by the vibrations of the beam itself, but also by the entire measurement setup. Furthermore, a comparison of the natural frequencies and mode shapes between the numerical model and the experiment showed considerable discrepancies resulting from difficulties in obtaining rigid support in the measurement stand. This issue was addressed by replacing the fixed support in the model with elastic constraints.

The research carried out has shown that mechanical metamaterials offer immense potential for shaping the mechanical parameters of structures, leading to their wide application, including in civil engineering. The flexibility of the metamaterial geometry allows for a significant influence on both the static and dynamic response of the structures, which is crucial in terms of their potential applications. In this study, we analysed structures that were not subjected to external loads. However, in future research, we will also focus on the dynamic behaviour of 3D printed beams under external loads.

## Acknowledgements

These studies were conducted with the financial support of the Gdańsk University of Technology by the DEC-7/2/2023/IDUB/III.1a/Ra grant under the RADIUM Learning Through Research Programs 'Excellence Initiative – Research University' program.

Computations were carried out using the computers of Centre of Informatics Tricity Academic Supercomputer & Network.

## REFERENCES

1. Evans K.E., Alderson A. Auxetic materials: Functional materials and structures from lateral thinking! *Advanced Materials*. 2000;12(9):617–28.
2. Tan X., Zhu S., Wang B., Kadic M. Tuning negative stiffness mechanical metamaterial's snap-through behavior with a series-connected spring. *European Journal of Mechanics, A/Solids*. 2024;107(May):105382.
3. Pendry J.B., Schurig D., Smith D.R. Controlling electromagnetic fields. *Science*. 2006;312(5781):1780–2.
4. Smith D.R., Schultz S., Markoš P., Soukoulis C.M. Determination of effective permittivity and permeability of metamaterials from reflection and transmission coefficients. *Physical Review B - Condensed Matter and Materials Physics*. 2002;65(19):1–5.
5. Sheng P., Zhang X.X., Liu Z., Chan C.T. Locally resonant sonic materials. *Physica B: Condensed Matter*. 2003;338(1–4):201–5.
6. Wu P., Mu Q., Wu X., Wang L., Li X., Zhou Y., et al. Acoustic absorbers at low frequency based on split-tube metamaterials. *Physics Letters, Section A: General, Atomic and Solid State Physics*. 2019;383(20):2361–6.
7. Zangeneh-Nejad F., Fleury R. Active times for acoustic metamaterials. *Reviews in Physics*. 2019;4(April):100031.
8. Shelby A.R.A., Smith D.R., Schultz S. Experimental verification of a negative index of refraction. *Science*. 2001;292(5514):77–9.
9. Wang K.X., Zhou E.L., Wei B.L., Wu Y., Wang G. An efficient and accurate numerical method for the heat conduction problems of thermal metamaterials based on edge-based smoothed finite element method. *Engineering Analysis with Boundary Elements*. 2022;134(August 2021):282–97.
10. Veselago V.G. The Electrodynamics of substances with simultaneously negative values of  $\epsilon$  and  $\mu$ . *Soviet Physics Uspekhi*. 1968;10(4):509–14.

11. Lakes R. S. Foam structures with a negative Poisson's ratio. *Science*. 1987;235(1987):1038–41.
12. Kadic M., Bückmann T., Stenger N., Thiel M., Wegener M. On the practicability of pentamode mechanical metamaterials. *Applied Physics Letters*. 2012;100(19).
13. Wang Z., hu H. Auxetic materials and their potential applications in textiles. *Textile Research Journal*. 2014;84(15):1600–11.
14. Neville R.M., Scarpa F., Pirrera A. Shape morphing Kirigami mechanical metamaterials. *Scientific Reports*. 2016;6(July):1–12.
15. Xiao D., Kang X., Li Y., Wu W., Lu J., Zhao G., et al. Insight into the negative Poisson's ratio effect of metallic auxetic reentrant honeycomb under dynamic compression. *Materials Science and Engineering: A*. 2019;763(July):138151.
16. Wang K., Wu C., Qian Z., Zhang C., Wang B., Vannan M.A. Dual-material 3D printed metamaterials with tunable mechanical properties for patient-specific tissue-mimicking phantoms. *Additive Manufacturing*. 2016;12:31–7.
17. Kolken H.M.A., Janbaz S., Leeflang S.M.A., Lietaert K., Weinans H.H., Zadpoor A.A. Rationally designed meta-implants: A combination of auxetic and conventional meta-biomaterials. *Materials Horizons*. 2018;5(1):28–35.
18. Krolkowski T., Knitter R., Blazejewski A. Computer modeling and testing of structural metamaterials. *Procedia Computer Science*. 2019;159(October):2543–50.
19. Zadpoor A.A. Mechanical performance of additively manufactured meta-biomaterials. *Acta Biomaterialia*. 2019;85:41–59.
20. Dogan E., Bhusal A., Cecen B., Miri A.K. 3D Printing metamaterials towards tissue engineering. *Applied Materials Today*. 2020;20:100752.
21. Yang H., Ma L. Design and characterization of axisymmetric auxetic metamaterials. *Composite Structures*. 2020;249(March).
22. Li S., Hou Y., Huang J., Shi J., Meng L. Exploring the enhanced energy-absorption performance of hybrid polyurethane(PU)-foam-filled lattice metamaterials. *International Journal of Impact Engineering*. 2024;193(April):105058.
23. Boldrin L., Hummel S., Scarpa F., Di Maio D., Lira C., Ruzzene M., et al. Dynamic behaviour of auxetic gradient composite hexagonal honeycombs. *Composite Structures*. 2016;149:114–24.
24. Mazloomi M.S., Ranjbar M., Boldrin L., Scarpa F., Patsias S., Ozada N. Vibroacoustics of 2D gradient auxetic hexagonal honeycomb sandwich panels. *Composite Structures*. 2018;187(August 2017):593–603.
25. Anigbogu W., Nguyen H., Bardaweel H. Layered metamaterial beam structures with local resonators for vibration attenuation: Model and experiment. *Frontiers in Mechanical Engineering*. 2021;7(October):1–13.
26. Pires F.A., Sangiuliano L., Denayer H., Deckers E., Desmet W., Claeys C. The use of locally resonant metamaterials to reduce flow-induced noise and vibration. *Journal of Sound and Vibration*. 2022;535(November 2021):117106.